AUTOMATIC DETECTION OF THREE RADIO-OPAQUE MARKERS FOR PROSTATE TARGETING USING EPID DURING EXTERNAL RADIATION THERAPY

Sébastien Pouliot[1,2], André Zaccarin[3], Denis Laurendeau[2] and Jean Pouliot[4]

1. Centre Hospitalier Universitaire de Québec, Hopital Hotel-Dieu de Québec
2. Computer Vision and Systems Lab., Université Laval, Quebec City, QC, Canada
3. Microprocessor Research Labs, Intel Corporation, Santa Clara, Ca. USA
4. University of California San Francisco, Department of Radiation Oncology

ABSTRACT

External radiotherapy is an option used for the treatment of the prostate cancer. In order to achieve the best results, radiation must be precisely delivered to the target volume while preserving healthy tissues and protecting organs at risk. Electronic Portal Imaging Devices (EPID) are now available to verify the dose delivery by using the treatment radiation to obtain a portal image. The localization of the prostate, usually not visible on portal images, is performed by inserting up to three radio-opaque markers into the prostate. The identification and position of the markers relative to bone structures and beam field are used to insure the proper delivery of radiation to the prostate. In this paper, we present a sequence of algorithms optimized for the automatic detection of the three radio-opaque markers on images obtained with EPID during prostate radiotherapy. Neural network is used to validate the detection of true markers in images.

1. INTRODUCTION

The recent implementation of new technologies, including patient immobilization devices, tomodensitometry based (CT) treatment planning, beam visualisation tools, 3D dose calculation and electronic portal imaging have improved the efficiency of prostate cancer treatment using external beam radiation. It has been demonstrated for several anatomical sites, including prostate, that increasing radiation dose to the tumor improves local tumor control and survival. This dose escalation can only be tolerated if it is achieved without increasing the dose delivered to normal tissues. This technique, called conformal therapy, is an exciting new development in the field of radiation therapy. The reduction of the volume receiving clinically significant doses of radiation raises the important issue of tumour targeting. The quality of the treatment of prostate cancer by radiation is strongly dependent on the ability to localize the target volume and to precisely deliver the planned dose.

External reference points can be used to properly align and immobilize the patient. Nerderveen *et al.* [1] put radio-opaque markers on a perspex template on the skin of the patient and used EPID to assess the proper positioning of bony structures. By implanting a radio opaque marker into the prostate and using EPID, Vigneault *et al.* [2] have shown large daily displacements of the prostate during the course of radiation therapy. They have measured marker displacements of up to 1.6 cm, stressing the importance to determine the position of the prostate before each irradiation. We now routinely use three radio-opaque markers implanted in the prostate under ultrasound guidance to verify the proper position of the beam field. The use of three markers instead of one also allows the investigation of organ distortion and rotation.

The markers create weak attenuation in the portal image (Girouard [3]). Their specific signature can be used to identify them among all other features observed on a portal image. In this paper, we present a sequence of algorithms for the automatic detection of the markers. The performance of the detection tool is evaluated on phantom and clinical images.

2. METHOD

The clinical images were obtained during the radiation therapy of patients treated for prostate cancer with a high energy beam (17 MeV) using a video-based EPID*. Figure 1 shows one of those images. Because of the high energy beam, these images are noisy and have poor contrast which makes the automatic detection of the radio-opaque markers a challenging problem. There are several algorithms for image processing enhancement and shape detection, but only some of these work well on the type of

---
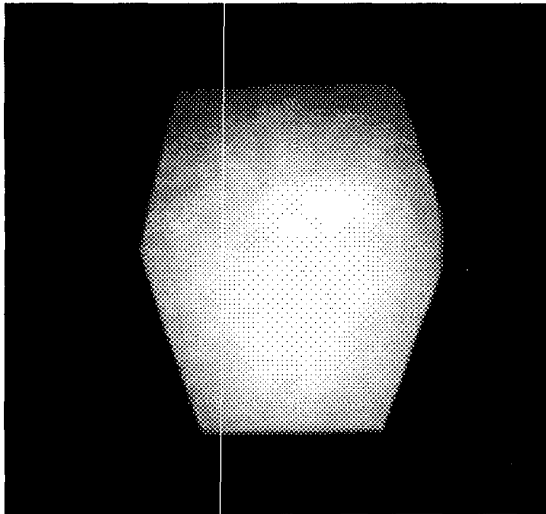
* BeamviewPLUS from Siemens Oncology Care Systems

Fig. 1. Clinical image.

2.1 Determining the search zone

2.2 Image enhancement

2.3 Local minimum   2.4 Creating the contrast image

2.5 Attenuation analysis

2.6 Detecting the markers by constellation
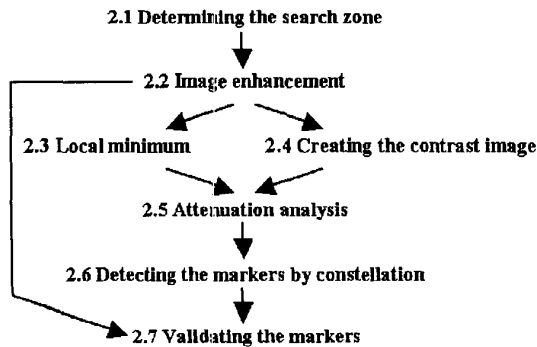
2.7 Validating the markers

Fig. 2. Steps of the algorithm.

image used. Furthermore, the time constraints for execution skewed the choice towards simple but effective algorithms.

First, we limit the search area using a priori information about the location of the markers. Local minima are then identified in the enhanced image, and a weight is given to each of these minimum based on the corresponding data in the contrast image. Finally, the markers are detected using a matching algorithm that uses the known geometry between the 3 markers. In the last step, we validate the detected markers using a geometrical model of the marker attenuation and a neural network classifier. Figure 2 illustrates the steps of the algorithm, which are described in the following sections.

2.1. Determining the search zone

Minimizing the search zone is a very significant step in finding the markers. The smaller the search zone, the faster the algorithm and the lower the risk of false detections. To determine the area of interest, the original positions of the markers for each field are extracted from a reference image. This image can be the simulation film, the DRR (digitally reconstructed radiograph from the CT scan), or the first EPID image acquired during the delivery of the first fraction of the dose.

Displacement of the prostate can reach up to 1.6 cm [2]. Thus, the area of interest is approximately 16 mm relative to the initial position of the markers. Also, there can be some difficulty when the area of interest includes part of the edge of the field. We erode the area of interest in order to eliminate this problem.

2.2. Image enhancement

Adaptive histogram equalization with limitation of contrast (CLAHE) [4] makes it possible to better distinguish the contours and the markers. After equalizing the histogram, we apply a uniform average filter of 3x3 to remove high-frequency noise.

2.3. Local minimum

The attenuation made by a marker creates a local minimum. Thus, processing speed is increased if only the local minima are treated. A pixel is considered to be a local minimum if it has the smallest value of a 5x5 window centered on it.

2.4. Creating the contrast image

The images are very different from one another. The average level of intensity where the markers are located differs significantly from one image to the other, and from one marker to the other in the same image. The use of a contrast image rectifies this situation.

The contrast image has to emphasize the attenuation of the parabolic shape. The contrast image *IContrast* is obtained in the following way:

$$IContrast = \frac{MCenter}{MRing} \qquad (2.1)$$

where *MCenter* is the average value of a circle of 7 pixels in diameter and *MRing* is the average value of a unit ring of 13 pixels in diameter. Only the zone found in section 2.1 is processed to accelerate the processing speed. The masks are circular because the ratio between the length and the diameter of our markers is too small for the marker orientation to be useful in the detection process. Nederveen *et al.* [1] use the orientation of the markers when searching for the markers, but the length of their markers is larger and the diameter is smaller.

2.5. Attenuation analysis

Using the contrast images, a weight must be associated with each local minimum found at step 2.3. The higher the weight of a minimum is, the greater the probability that the minimum will be a marker. The weight of the minimum is determined by the average decrease in pixel intensity over the minimum with respect to the intensity plane in which this minimum lies.
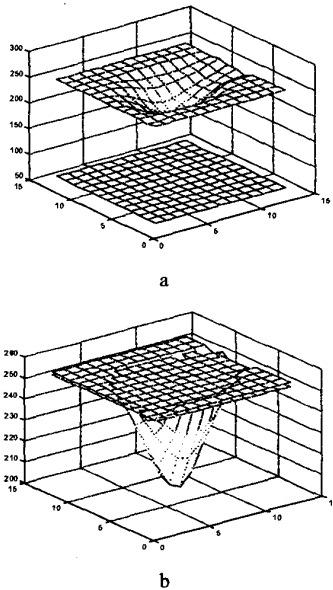
858

a

b

Fig. 3. Covering the attenuation by a plane. (a) A parallel plane is found and (b) the offset is adjusted to cover the attenuation.

a

b

Fig. 4. Modelling of the attenuation by a quadric. (a) The attenuation and (b) the modelling by a quadric.

Using the method of least squares, we determine a parallel plane with the average orientation of a window of 13x13 pixels centered on the minimum currently being processed. By using the unit ring centered on this minimum, we can adjust the offset of the plane to cover the attenuation. Figure 3 illustrates the attenuation covering by a plane.

The weight that we associate with each local minimum is described as follow:

$$W = \sum_{circle} (Z2 - I) \qquad (2.2)$$

where W is the weight, Z2 is the adjusted plane, and I is the matrix of the intensities of the image. The summation is done on a circle of 11 pixels in diameter centered on the local minimum.

2.6. Detecting the markers by constellation

The markers are at a certain distance from one another. This constellation can be useful for detecting the group of three markers. The initial position of the markers is already known (see 2.1). According to Hai *et al.* [5], displacement between the markers can go up to 4 mm based on the average position of the markers. Since we use the initial positions of the markers, this displacement can be larger than 4 mm. In practice, the use of a displacement of approximately 6 mm yields good results.

The initial position of the three markers for each field of the treatment is therefore known within a certain tolerance defined by the organ motion. For each local minimum found in Section 2.3, the marker is assumed to
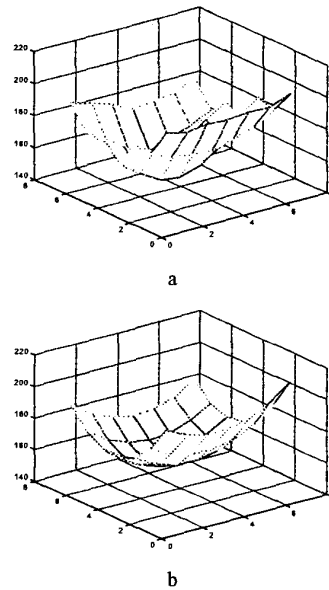
be the central marker. Two search windows are then used to associate a weight with this local minimum. The center of each window depends on the relative distance between the original position of the central marker and the two other markers. The width of each window is approximately 6 mm. However, it is important that the windows not overlap. The two windows remain at the same relative position from each other and move when the local minimum being processed changes.

The superior and inferior markers are chosen as those having the greatest value in the search windows. These are the values found in section 2.5. Since only the local minima were treated in section 2.5, the values of the other points are equal to zero. When all the local minima have been processed, we take the one with the greatest value. This is the value most likely to represent the three markers.

2.7. Validating the markers

At this point, the detection of the markers is finished. Given the poor quality of the images, it can happen that the detected markers are not the right ones. Therefore, we have developed a test to increase the reliability of detection. This test is based on the search for the radio-opaque marker of Girouard [3].

The attenuation made by a marker can be modeled with a quadric (figure 4). Here again, the least square method is used. For each of the three markers found, we do a modeling with the quadric. We establish three Hessian matrices for each quadric. Each matrix has two eigenvalues: x1 and x2. The smallest x1 and x2 are

used as input by a perceptron. The perceptron separates good detections from bad detections. The goal is to keep the good detections while having the least possible number of bad detections accepted.

3. RESULTS

3.1. Experimental conditions
The algorithm was tested on 109 images from 5 patients at the Centre Hospitalier Hôtel-Dieu in Quebec City (HDQ) and 216 images from 2 patients of the University of California San Francisco (UCSF). The HDQ images were taken with 3 different cameras involving some variations in the quality and characteristics of the images. The UCSF images were taken with 2 different cameras. Also, one of the UCSF patients had only 2 markers.

3.2. Experimental Results
The detection efficiency values can be separated in two categories, one for the detection of each marker individually and another category for the global detection of a group of three markers. For the individual detection, the efficiency values are 98%, 94% and 63% for antero-posterior, oblique and lateral fields, respectively. The average detection efficiency is 84%. For the same beam incidence angles, the global detection efficiency values of a group of three markers are 96%, 83% and 51% respectively (average 77%). These results are given in Table 1.

In an attempt to provide the user with a confidence level, a neural network was trained to evaluate the proper detection of the markers. For all angles and markers, the number of false positive remained less than 3%. Table 2 shows the results after validation for the detection of all markers in an image.

3.3. Execution time
The execution time of the algorithm varies from 20 to 40 hundredths of a second. This time is a function of the position of the markers. The greater the space between the markers is, the greater the size of the area to be processed, and thus, the longer the execution time. The algorithm was executed on a Pentium II 400 MHz with 64MB of RAM.

4. DISCUSSION AND CONCLUSION

A sequence of algorithms to perform the automatic detection of radio-opaque markers were developed and tested on clinical electronic portal images. The detection efficiency is very high (98%) for antero-posterior field. The efficiency decreases while the beam incident angle increases, reaching its minimum efficiency (63%) at 90 degrees.

FIELD OF VIEW	INDIVIDUAL MARKERS	GROUP OF MARKERS
AP/PA	98%	96%
OBLIQUE	94%	83%
LATERAL	63%	51%

TABLE 1. Detection rate before validation

FIELD OF VIEW	TRUE POSITIVE	FALSE POSITIVE	TRUE NEGATIVE	FALSE NEGATIVE
AP/PA	90%	1%	3%	6%
OBLIQUE	53%	3%	14%	30%
LATERAL	20%	2%	47%	31%

TABLE 2: Detection rate after validation

The major difficulty in detecting markers comes from the high noise level present in the image, in particular for low intensity lateral (90 degrees) images. Although the detection efficiency is high on average and false positive are rare (less than 3%), there is room for improvement. It is probable however that better detection efficiencies will be obtained with the evolution of the cameras used, in particular with the integration mode video camera, known for their high sensitivity and low noise.

The use of a confidence level determined from the application of a neural network will contribute to the acceptation of computer assisted decision making on the proper position of the treated organ. The execution speed of the algorithm presented here will allow quasi-real time localization of the prostate for the proper targeting of the organ during radiation delivery.

5. REFERENCES

[1] A. Nederveen *et al.*, "Detection of fiducial gold for automatic on-line megavoltage position verification using a marker extraction kernel (MEK)", Int. J. Radiation Oncology Biol. Phys., vol. 47, no. 5, pp. 1435-1442, 2000.

[2] E. Vigneault *et al.*, "Electonic portal imaging device of radioopaque markers for the evaluation of prostate position during megavoltage irradiation : a clinical study", Int. J. Radiation Oncology Biol. Phys., vol. 37, no. 1, pp. 205-212, 1997.

[3] L.-M. Girouard, "Imagerie portale en radiothérapie :Localisation automatique de la prostate", Mémoire de maîtrise, november 1996.

[4] S. M. Pizer, "Adaptive histogram equalization and its variations", Computer Vision, Graphics, And Image Processing 39, pp. 355-368, 1987.

[5] J. Hai *et al.*, "A clinical study of prostatic motion during radiation treatment with the use of EPID and radioopaque markers", Department of Radiation Oncology, UCSF, San Francisco, CA 94143-0226.